PCCP

Accepted Manuscript

ROYAL SOCIETY OF CHEMISTRY

www.rsc.org/pccp

PCCP

ARTICLE

Growth of 3D hierarchical porous NiO@Carbon nanoflakes on graphene sheets for high-performance Lithium-ion batteries

Received 00th January 20xx,
Accepted 00th January 20xx

DOI: 10.1039/x0xx00000x

www.rsc.org/

Xiongwei Wang[a,‡], Ludan Zhang[b,‡], Zehui Zhang[a], Aishui Yu[b], Peiyi Wu[a,*]

Nickel oxide (NiO), as one of the anode electrode materials for Lithium ion batteries (LIBs) has attracted considerable research attention. However, the poor electron conductivity and bad capacity retention performance greatly hinder its wide application. Herein, we prepared a novel three-dimensional (3D) hierarchical porous graphene@NiO@Carbon composite via simple solvothermal process, in which the graphene sheets were uniformly wrapped by porous NiO@Carbon nanoflakes. In this case, nickelocene was creatively used as the precursor for both NiO and amorphous carbon, while graphene oxide sheets were employed as a template for the two-dimensional nanostructure and conductive graphene backbone. The resultant composites possess high surface area (196 $m^2 g^{-1}$) and large pore volume (0.46 $cm^3 g^{-1}$). When it is applied as an anode for LIBs, the carbon out-layer can effectively suppress the large volume change and serious aggregation of NiO nanoparticles during the charge-discharge process. Therefore, the graphene@NiO@Carbon composites show a high reversible capacity of 1042 mAh g^{-1} at a current density of 200 mA g^{-1}, excellent rate performance and long cycle life. We believe that our method provide a new route to fabricate novel transition metal oxide composites.

1. Introduction

With the fast development of human society, there is a substantially increasing requirement for efficient and clean energy conversion and storage, especially in the consideration of issues like environment pollution and energy shortage.[1-3] Consequently, the enthusiasm for research on high-performance energy storage devices is rapidly growing in the past few decades.[4] Among these storage devices, Lithium ion batteries (LIBs), as a fast-developing technology in electric energy storage area, have attracted great attention because of its high energy density, long cycle life and environmental benignity.[5-9] However, as a commercial anode material in LIBs, graphite shows low theoretical capacity (372 mAh g^{-1}) and poor rate capability, which can not meet the increasing need of energy storage for various technological applications such as communication apparatus, electric vehicles, locomotives, and aerospace applications.[10-16] Therefore, it is essential to develop the next-generation LIBs with higher energy density and longer cycle life.

Recently, transition metal oxides, such as NiO, SnO_2, Fe_3O_4, TiO_2 and Co_3O_4, have been proposed as one of the most promising anode materials due to their high specific capacity and volumetric energy density.[13, 14, 17-19] Among these transition metal oxides, NiO emerges as a promising anodic materials for LIBs owing to its merits of natural abundance, low cost, environmental safety and high theoretical capacity (718 mAh g^{-1}).[20-25] Unfortunately, the low electronic conductivity and significant volume change during the lithiation-delithiation process always bring about poor rate performance and fast capacity fading.[23, 26-28] To circumvent these problems, one strategy is to synthsize NiO with various kinds of topological structure including nanoparticles,[29] nanofibers,[30] nanotubes,[31] nanoflakes[32] and hollow micro-spheres,[33] while the another strategy is to form composites by hybridizing with carbonaceous materials like graphene and carbon nanotube.[23, 34] In particularly, hollow or porous structure can effectively enhance the electrochemical performance by shortening the lithium ion diffusion distances and enlarging the surface area.[21, 26, 34] Besides, It is worth noting that coating metal oxide with amorphous carbon layer can not only suppress the large volume change and serious aggregation of metal oxide during charge-discharge process, then leading to an improvement of LIBs, but also act as crosslinker to bind metal oxide on conductive substrate.

Design and synthesis of three-dimensional (3D) hierarchical porous electroactive nanostructured materials grown directly on graphene sheets or CNTs are of great interest. By constructing 3D nanostructure, it can enlarge the contact areas between the materials and the electrolyte to facilitate Li^+ ion transport, and simultaneously the free space within

[a] State Key Laboratory of Molecular Engineering of Polymers, Collaborative Innovation Center of Polymers and Polymer Composite Materials, Department of Macromolecular Science and Laboratory for Advanced Materials, Fudan University, Shanghai 200433, P. R. China. E-mail: peiyiwu@fudan.edu.cn
[b] Department of Chemistry, Shang hai key laboratory of Molecular Catalysis and Innovative Materials, Collaborative Innovation Center of Chemistry for energy Materials, Institute of New Energy, Fudan University, Shanghai 200438, P. R. China.
‡These authors contributed equally to this work.
†Electronic Supplementary Information (ESI) available: FESEM and TEM images; EDX spectrum; high resolution XPS spectra; rate performance. See DOI: 10.1039/x0xx00000x

nanostructure can partially buffer the volume change of metal oxide during charge-discharge cycles.[23, 35, 36] So far, many works about the direct growth of various NiO nanostructures on conductive substrates have been reported.[22, 25, 37] However, few researchers have ever reported a composite with carbon coated NiO nanoparticles loaded on conductive substrate for the application in LIBs application.

Herein, we fabricated a 3D hierarchical porous graphene@NiO@Carbon composite through one-pot solvothermal method, in which the graphene sheets were uniformly wrapped by porous NiO@Carbon nanoflakes. And the obtained NiO@Carbon nanoflake was further constructed of carbon coated NiO nanoparticles. In this case, we creatively used nickelocene as the precursor for both NiO and amorphous carbon, while graphene oxide (GO) was utilized as a template for the growth of NiO and its reduced state, graphene, can provide fast electron conduction. The anchored density of NiO@Carbon nanoflakes on graphene sheets can be well tuned by changing the initial ratio of nickelocene to GO. Furthermore, the resultant graphene@NiO@Carbon composites manifest a high surface area of 196.0 m^2/g and a large pore volume of 0.46 cm^3/g. When used as anode material for LIBs, the graphen@NiO@Carbon composites show a high reversible capacity of 1042 mAh g^{-1} (at a current density of 200 mA g^{-1}), a good Coulombic efficiency of ~100 %, and an excellent rate performance.

2. Experimental Section

2.1 Materials

KNO3, concentrated H2SO4, KMnO4 and tetrahydrofuran were purchased from Shanghai Chemical Corp. Nickelocene was purchased from Aladdin and graphite power was provided by Sigma–Aldrich. Tetrahydrofuran was distilled over CaH2 prior to use, while the other chemicals were used as received without further purification. Deionized water was used for all experiments.

2.2 Synthesis of graphene@NiO@Carbon and NiO@Carbon

Graphene oxide (GO) was synthesized from natural graphite powers via a modified Hummers method.[38] Briefly, graphite (5.0 g) was added into a solution of concentrated H_2SO_4 (115 mL) cooled in an ice-water bath. KNO_3 (2.5 g) and $KMnO_4$ (15 g) were added very slowly (with a period more than 15 min) into the mixture. All the operations were carried out very slowly in a fume hood. The solution was allowed to stir in an ice-water bath for 2 h, then at 35 ^{o}C for 1 h. Afterwards, 115 mL of water were added to the flask. After 1 h, 700 mL of water were added. After 15 minutes, the solution was removed from the oil bath and 50 mL of 30% H_2O_2 were added to end the reaction. This suspension was stirred at room temperature for 5 minutes. The suspension was then repeatedly centrifuged and washed twice with 5% HCl solution and then dialyzed for a week.

The graphene@NiO@Carbon composites were prepared by a one-pot solvothermal method. In a typical process, GO were transferred from the aqueous suspension into anhydrous tetrahydrofuran by centrifugation. Different amount of nickelocene (0.045, 0.075, 0.105, and 0.135 g) was fully dissolved in 8 mL anhydrous tetrahydrofuran with intense sonication for 10 min. Subsequently, 2 mL GO tetrahydrofuran (7.5 mg/mL) suspension was added into the above solution. The mixture solution was further sonicated for another 30 min. After that, the precursor solution was transferred to a Teflon lined stainless autoclave and then heated in an oven at 210 °C for 24 h. After 24 h, the autoclave was cooled to room temperature naturally. Black product was collected by centrifugation and washed with absolute ethanol for several times. The as-obtained powders were dried at 60 °C overnight. Finally, the resultant samples were put into a quartz tube and calcined at 320 °C in air for 2.5 h to improve the crystallinity. The NiO@Carbon nanoflowers were prepared via a similar solvothermal method as described above without GO sheets.

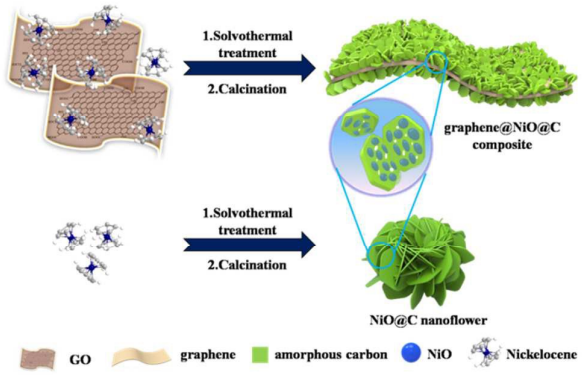

Fig.1 Schematic illustration of the formation mechanism of graphene@NiO@C composites and NiO@C nanoflowers

2.3 Electrochemical Tests

The working electrodes were prepared by dispersing 85 wt% as-prepared composites, 5 wt% Super P carbon black, and 10 wt% polyvinylidene difluoride (PVDF) binder in N-methyl-2-pyrrolidinone (NMP). And then the mixture slurry was pasted onto a copper foil current collector. Before pressing, the electrodes were dried at 80 °C for 12 h in vacuum oven to remove the solvent. The electrodes were punched in the form of disks (diameter: 12 mm and weight: 5 mg) and then vacuum-dried at 80 °C for 24 h. The electrolyte solution was 1 M LiPF6 in ethylene carbonate (EC) and diethyl carbonate (DEC) (1: 1 by volume). The cells were assembled with the as-prepared positive electrode, lithium metal, and separators (Celgard 2300 film). The cell assembly was operated in a high purity-argon filled glove box. Cyclic voltammetry (CV) and electrochemical impedance spectra (EIS) were conducted on a CHI660C electrochemistry workstation. CV test was carried out in the voltage range of 0.01-3.0V (vs Li^+/Li) at a scan rate of 0.1 mV s^{-1}. EIS experiment was carried out with a frequency loop from 10^5 Hz to 0.1 Hz at an amplitude of 5 mV versus the open circuit potential. The galvanostatic charge-discharge measurements were performed on LAND test system (LAND

CT2001A model) at different current densities with the voltage range of 0.01-3.0 V for half cells.

2.4 Characterization

Field-emission scanning electron microscopy (FESEM) was performed on Zeiss Ultra 55 with EDX. Transmission electron microscopy (TEM) experiments were conducted on JEOL JEM2011 F Microscope (Japan) operated at 200 kV. The samples for the TEM measurements were dispersed in ethanol and then supported onto a holey carbon film on a Cu grid. Atomic force microscope (AFM) images were obtained using a Bruker Multimode 8 (Germany) in the tapping mode. The samples were deposited on a freshly cleaved mica surface by spin coating. Nitrogen sorption isotherms were measured at 77 K with a Micromeritcs Tristar 3020 analyzer. The pore size distributions (PSD) were derived from the adsorption branch of the isotherms using the Barrett-Joyner-Halenda (BJH) model. XRD patterns were recorded on X'pert PRO PANalytical (Netherland) with Ni-filtered Cu Kα radiation (40 kV, 40 mA). Thermogravimetric analysis (TGA) was conducted on a Metter Toledo TGA 1 (Switzerland) from 100 to 800 °C in air with a heating rate of 10 °C/min. The Raman spectrum was obtained using HORIBA XploRA (France).

3. Results and discussion

3.1 Structural and compositional characterizations

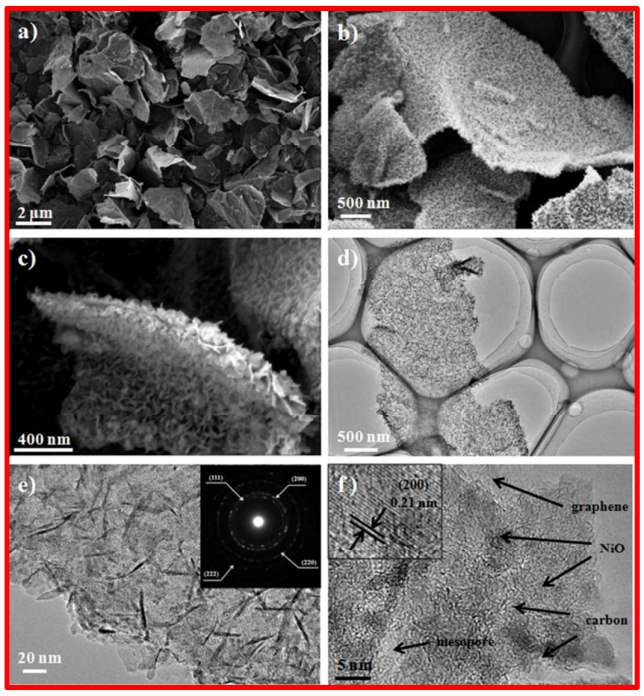

Fig.2 SEM (a-c) and TEM (d and e) images of graphene@NiO@C composites. Inset in (e) presents the selected area electron diffraction pattern. (f) High resolution TEM image of graphene@NiO@C composites

The formation mechanism of graphene@NiO@Carbon (denoted as graphene@NiO@C below) composite and NiO@Carbon (denoted as NiO@C below) nanoflower are described in Fig. 1. After solvothermal process, porous NiO@carbon nanoflakes were anchored on GO sheets via the hydrolysis of nickelocene in THF at 210 °C. The real morphology of the prepared graphene@NiO@C composites are first studied by Field emission scanning electron microscopy (FESEM). FESEM images of the resulting graphene@NiO@C composites in Fig. 2a,b reveal that the free-standing graphene sheets are densely and uniformly wrappedby many NiO@C nanoflakes. The magnified FESEM image in **Fig. 2**c clearly discloses that these ultrathin nanoflakes randomly interconnect with each other on both of the graphene surfaces to form 3D nanostructure with lots of free space between adjacent nanoflakes. These free space are beneficial for reducing the structural stress during charge-discharge process.[23, 27, 39] However, in the absence of GO, NiO@C nanoflakes tend to self-assemble into nanoflowers with sizes ranging from 400 nm to 800 nm (Fig. S2a). Interestingly, as shown in the magnified image in Fig. S2b, the surface of the NiO@C nanoflakes is very rough, which implies that the NiO@C nanoflakes may be further composed of smaller nanoparticles. This conjecture is confirmed by the Transmission electron microscopy (TEM) images in Fig. S2c,d that the NiO@C nanoflakes are indeed constructed of carbon coated NiO nanoparticles, which suggests that the NiO core is firstly formed during the hydrolysis of nickelocene, then the hydrothermal carbonization of cyclopentadienyl species is triggered into the outer carbon shell. TEM images of graphene@NiO@C composites (Fig. 2d and Fig. S3a,b) notably show that a large number of NiO@C nanoflakes are densely loaded on graphene sheets, which is consistent with the FESEM results. Furthermore, the rough surface of the NiO@C

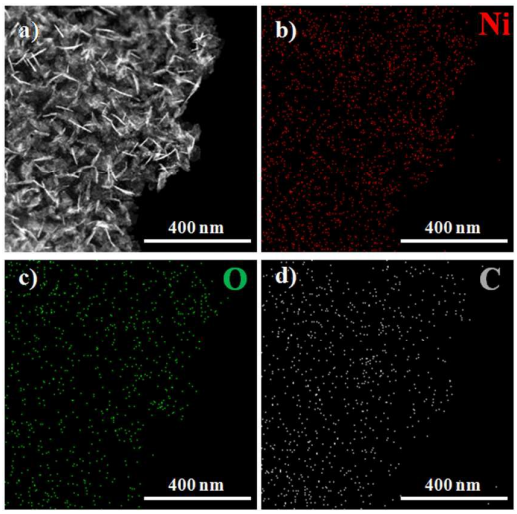

Fig.3 STEM image of graphene@NiO@C sheets (a) and the corresponding EDX element mapping of Ni, O, C at the region in (a), respectively (b-d).

nanoflakes can also be observed in Fig. 2e. The selected area electron diffraction (SAED) pattern (Fig. 2e inset) obviously presents four well-resolved diffraction rings, which can be indexed to the (111), (200), (220) and (222) planes of NiO in the face-centered cubic phase, suggesting the existence of NiO on the graphene sheets. X-ray spectroscopy (EDS) analysis (Fig. S4) further confirms the presence of C, O and Ni elements in the graphene@NiO@C sheets, while Cu peak originates from the copper grid supporting the sample. HRTEM image (Fig. 2f) distinctly manifests that the NiO@C nanoflakes are assembled by many highly crystalline NiO nanoparticles which are coated by ultrathin carbon layer, and the crystalline lattices (Fig. 2e inset) with a d spacing of 0.21 nm corresponds to (200) plane of NiO. Additionally, some mesopores can be observed on the NiO@C nanoflakes, which are mainly caused by the stacking of adjacent NiO@C nanoparticles. These mesopores may provide extra space for lithium storage as well as shorten the lithium ions diffusion length.[36, 39, 40]

Moreover, the uniform distribution of NiO@C nanoflakes on graphene sheets are further elucidated by scanning TEM image (Fig. 3a). The corresponding element mapping of Ni, O and C in Fig. 3b-d also confirms the uniform dispersion of NiO nanoparticles on graphene sheets and the conformal coating of the ultrathin carbon layer. Atomic force microscopy (AFM) analyses (Fig. S5a,b) further confirm the 3D feature of graphene@NiO@C composites with an average thickness of ~50 nm, and a rough surface, which is well in agreement with the above FESEM and TEM images.

X-ray diffraction (XRD) pattern of the graphene@NiO@C composites is depicted in Fig. 4a. All the characteristic peaks of (111), (200), (220), (222) and (311) planes can be well indexed to cubic NiO (JCPDS No. 071-1179). Additionally, a wide diffraction peak located at ~25° is the typical (002) plane of carbonaceous materials.[41, 42] Raman spectroscopy is a most common method that can be used to characterize graphitic materials. In addition to the characteristic peaks of carbonaceous materials at ~1590 cm^{-1} (G band, originating from the in-plane stretch vibration of carbon atoms) and ~1350 cm^{-1} (D band, originating from the breathing vibration of carbon atoms), one can also see the characteristic peak of NiO at ~500 cm^{-1}, indicating the existence of NiO in graphene@NiO@C composites (as shown in Fig. 4b).[39, 43] Moreover, the wider D band and G band of NiO@C imply the low graphitic degree of carbon outerlayer. XPS spectrum presented in Fig. 4c obviously shows the C 1s, O 1s and Ni 2p peaks in graphene@NiO@C composites. In addition, the high-resolution C1s spectrums of graphene oxide (GO) and graphene@NiO@C composites confirm that the GO sheets have been effectively reduced during solvothermal and subsequent calcination (Fig. S6a,b).

Nitrogen adsorption/desorption isotherm and pore-size distribution curves are shown in Fig. 4d and Fig. S7ab. The Brunauer-Emmett-Teller (BET) specific surface areas of graphene@NiO@C composites and NiO@C nanoflowers are calculated to be 196 $m^2 g^{-1}$ and 162 $m^2 g^{-1}$, respectively. The pore volume of graphene@NiO@C composites is ~0.46 $cm^3 g^{-1}$,

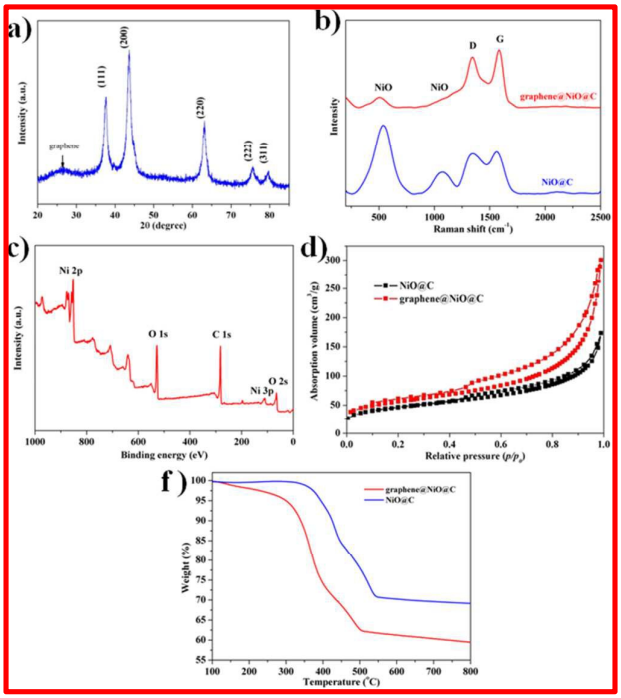

Fig.4 (a) XRD pattern, (b) Raman spectrum and (c) XPS spectrum of graphene@NiO@C composites. (d) Nitrogen adsorption/desorption isotherms and (e) TGA curves of graphene@NiO@C composites and NiO@C nanoflowers.

which is obviously larger than NiO@C nanoflowers(0.27 $cm^3 g^{-1}$), while the size of mesopores of these two materails all mainly distributes around ~3.6 nm. The higher pore volume of graphene@NiO@C is mainly ascribed to that graphene can suppress the aggregation of NiO@C nanoflakes. Moreover, the weight fraction of NiO in the resultant graphene@NiO@C composites and NiO@C nanoflowers were detected by TGA. Carbon (including graphene carbon and amorphous carbon) will be completely burn out under the circumstance of air when heated to 800 °C. It is assumed that the nickelocene is consistently transformed into NiO and carbon. Thus the weight fraction of NiO and graphene in the graphene@NiO@C composites can be estimated to be ~59.5 wt% and ~14.0 wt%, respectively.

The influence of the initial ratio of nickelocene to GO on the morphology of the resultant composites was also investigated. At low nickelocene concentration (0.045 g), NiO@C nanoflakes are sparsely loaded on the graphene sheets (Fig. S8a). HRTEM image (Fig. S8b) shows that aggregated NiO nanoparticles are also highly crystallized and coated by amorphous carbon shell. With the increase in the nickelocene concentration (0.075 g), the loading density of NiO@C nanoflakes anchored on graphene sheets is obviously increased (Fig. S8c). When the nickelocene concentration rises to 0.135 g (Fig. S8d), the graphene@NiO@C sheets can also be obtained, however, free aggregated NiO@C nanoparticles are concurrently formed. These results can be further confirmed by the corresponding FESEM images in Fig. S9. Therefore, one can obtain uniform

and perfect graphene@NiO@C composites and simutaneously easily regulate the loading density of NiO@C nanoflakes by rationally controlling the adding amount of nickelocene.

3.2 Electrochemical performance

Cyclic votalmmograms (CV) tests and galvanostatic discharge/charge measurements were first investigated in half-cell configurations to assess the lithium storage properties of the as-prepared graphene@NiO@C composites as an anode electrode in LIBs. Pristine NiO@C nanoflowers, as the reference, were also tested by the same electrochemical conditions. Fig. 5a shows the CV curves of the graphene@NiO@C composites for the first two cycles. In the first cycle, the characteristic cathodic peak located at ~0.4 V is corresponding to the initial reduction of NiO to Ni accompanied by the formation of amorphous Li_2O and partically irreversible solid electrolyte interphase (SEI) layer.[22, 23, 44] However, this reduction peak shifts to ~0.9 V and becomes smaller at the second cycle. In addition, two anodic peaks are observed around 1.35 V and 2.25 V during the first charge process, which correspond to the partial decomposition of SEI layer and the conversion of Ni to NiO according to the equation of $Ni+Li_2O \rightarrow 2Li+NiO$, respectively.[25, 45]

Fig. 5bc displays the first and second charge-discharge voltage profiles of graphene@NiO@C composites and NiO@C nanoflowers at a current density of 200 mA g^{-1}. Consistent with the above CV behavior, the first discharging curve shows a potential plateau at approximatelly 0.6 V due to the reduction of NiO to Ni and the formation of SEI layer.[27, 34] This potential plateau becomes steeper and shifts up to a scope from 0.8 V to 1.1 V in the following cycle, which is similar to the previous reports.[23-26] While the potential slopes at about 1.35 V and 2.25 V in the charge process are originated from the decomposition of SEI film and the oxidation of Ni to NiO.[24, 29] As a result, a high capacity of 1490 mAh g^{-1} and 1035 mAh g^{-1} can be delivered for the first discharge and charge process, respectively, and the corresponding initial Coulombic efficiency is about 69.4 %. The initial discharge and charge capacity of NiO@C nanoflowers are 1225 mAh g^{-1} and 1020 mAh g^{-1}, respectively. Obviously, the initial capacities of these two materials are all much larger than the theoretical value of NiO (718 mAh g^{-1}). Nevertheless, the discharge capacity of graphene@NiO@C composites is reduced to 1040mAh g^{-1} in the second cycle, giving rise to a irreversible loss of about 30 %. The excess discharge capacity can be mainly derived from the formation of solid electrolyte interphase (SEI) layer, bacause these polymeric gel-like films originated from electrolyte decomposition can provide extra lithium storage.[18, 22, 27, 46] Additionally, Ding et al believe that the lithium storage from the interfacial charging mechanism under electromotive force can also make some contribution to the excess capacity.[23, 47]

Fig. 5d demonstrates the cycling performance of graphene@NiO@C composites and NiO@C nanoflowers at a current density of 200 mA g^{-1}. It is clear that the cycling performance of graphene@NiO@C composites are superior to that of pristine NiO@C nanoflowers. The reversible capacity of NiO@C nanoflowers fades fast from 1030 mAh g^{-1} down to 598 mAh g^{-1} up to 20 cycles. In contrast, the graphene@NiO@C composites can still retain a high capacity of 754 mAh g^{-1} after 50 cycles, which is higher than the theoretical capacity of NiO (718 mAh g^{-1}). Besides, the Coulombic efficiencies are invariably approach to 100 % during 2 to 50 cycles, indicating excellent reversible capacity and cycling stability. The graphene sheets with high electron conductivity is responsible for the improvement of cycling performance of graphene@NiO@C composits. On the other hand, graphene sheets can not only buffer the volume change upon cycling by controlling the growth of NiO to form 3D nanostructure, but also partly prevent the aggregation of active materials.[22-24]

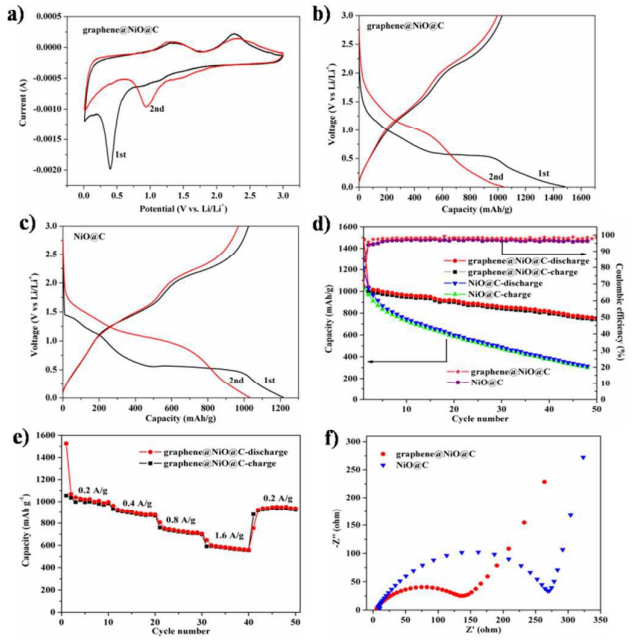

Fig.5 (a) cyclic voltammograms of graphene@NiO@C composites at a scan rate of 0.1 mV s^{-1} for the first and second cycle. Charge-discharge voltage profiles of graphene@NiO@C composites (b) and NiO@C nanoflowers (c) at a current density of 200 mA g^{-1}. (d) cycling performance of graphene@NiO@C composites and NiO@C nanoflowers at a current density of 200 mA g^{-1}. (e) rate performance of graphene@NiO@C composites at different current densities. (f) Nyquit plots of graphene@NiO@C composite and NiO@C nanoflower electrodes

To evaluate the rate capability of graphene@NiO@C composites and NiO@C nanoflowers, the electrodes were cycled under various current densities from 200 to 1600 mA g^{-1} and the results are presented in Fig. 5e and Fig. S10. As the current density is enhanced gradually from the initial 200 mA g^{-1} to 400 mA g^{-1}, 800 mA g^{-1} and 1600 mA g^{-1}, the graphene@NiO@C composites deliver an average discharge capacity of ~1015 mAh g^{-1}, ~883 mAh g^{-1}, ~721 mAh g^{-1} and ~580 mAh g^{-1}, respectively, which are all higher than that of NiO@C nanoflowers. It indicates the good rate performance for high power LIBs anode. When the current density is

returned to 200 mA g^{-1}, the capacity of graphene@NiO@C composites can be resumed to about 945 mAh g^{-1} for the next 10 cycles, suggesting a high reversibility and excellent rate capability. While for the NiO@C nanoflowers, the capacity is just resumed to about 430 mAh g^{-1}. Fig. 5f demonstrates the electrochemical impedence spectroscopies (EIS) of graphene@NiO@C composites and NiO@C nanoflowers before charge-discharge cycle. The Nyquist plots show that the charge transfer resistance (R_{ct}) of graphene@NiO@C composites is much smaller than that for the NiO@C nanoflowers. It implies that the highly conductive graphene sheets can facilitate the fast charge carrier transport during the charge-discharge process and thereby improve the rate performance.[18, 21, 24, 42] The cycling performance and rate capabilities of 3D hierarchical graphene@NiO@C composites can been comparable to many previous reported NiO-graphene compites (Table S1**).**

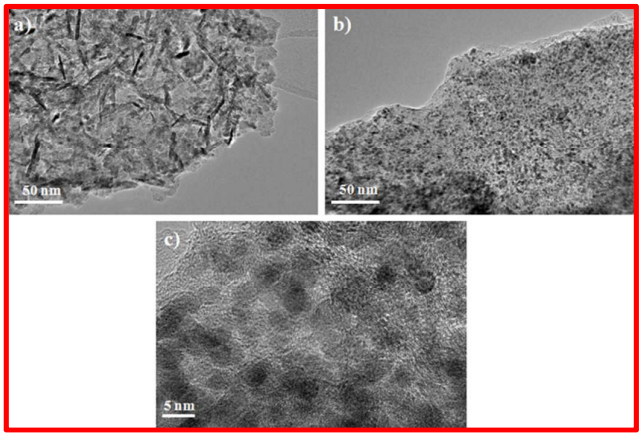

Fig.6 TEM images of graphene@NiO@C composites after different discharge-charge cycles: (a) after 10 cycles, (b,c) after 50 cycles.

The morphology and nanostructure of the graphene@NiO@C electrode after different discharge-charge cycles are also investigated. Fig 6a shows that the morphology of graphene@NiO@C composites generate a slight change after 10 discharge-charge cycles. However, after 50 dischrarge-charge cycles, the pristine morphology has been completely changed (Fig. 6b). While the NiO@C nanoparticles are still homogeneously dispersed on the graphene sheets and encapsulated within the carbon shell, with those of size up to ~6 nm. No large aggregated nanoparticles are observed, indicating that the outer carbon shell can well confine and stabilize the NiO nanoparticles on graphene sheets during cycling.

Fig. 7 outlines the proposed electron transfer and lithium ion diffusion mechanism during the lithiation-delithiation process. The reasons for the good electrochemical performance can be explained in the agruments below. First, the graphene sheets with high conductivity can enhance the electron transfer between the active materials and the current collector, relieve the aggregation of NiO@C nanoflakes and partially buffer the volume change of NiO, thus endow the electrode materials with good rate capability.[22-25, 28, 48] Second, the small size of NiO nanoparticles and the 3D hierarchical nanostructure with mesopore on NiO@C nanoflakes can not

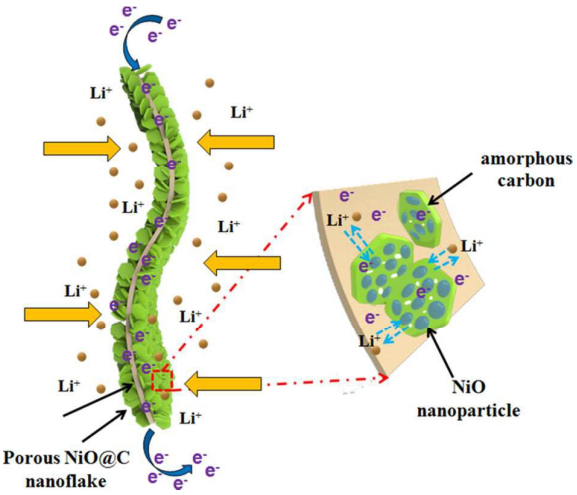

Fig.7 Schematic illustration of lithiation-delithiation process of graphene@NiO@C composites

only significantly buffer the large volume change of NiO nanoparticles but also shorten the Li ion diffusion path, which can greatly increase the lithium storage perporties and lithium solid solubility.[27, 36, 49, 50] Third, the uniform and elastic amorphous carbon outerlayers can effectively hinder the aggregation of NiO nanoparticles and assist the graphene to transfer electron, simultaneously as a binder to fix NiO nanoparticles on graphene sheets, resulting in good cycling stability of graphene@NiO@C composites.[18-21] Lastly, the large interfacial area can provide more sites for lithium ions storage as well as facilitate the Li^+ transfer between electrode and electrolyte.[5, 41]

4. Conclusions

In summary, we have successfully prepared a 3D hierarchical graphene@NiO@C composites through a one-pot solvothermal method. Nickelocene was creatively used as the precursor for both NiO and carbon to achieve in situ growth of porous NiO@C nanoflakes on graphene sheets, and the NiO@C nanoflakes are further consisted of carbon-coated NiO nanoparticles. The as-prepared graphene@NiO@C composites exhibited a high surface area of ~196 m^2 g^{-1} and a large pore volume of ~0.46 cm^3 g^{-1}. Moreover, the loading density of NiO@C nanoflakes on graphene sheets was greatly dependent on the initial ratio of nickelocene to GO. When investigated as anode materials for lithium-ion batteries, the graphene@NiO@C composites showed a high discharge capacity of 1040 mAh g^{-1} at a current density of 200 mA g-1, and the discharge capacity can also retain 754 mAh g^{-1} after 50 cycles. The good LIBs performance was also reflected in the excellent rate performance. The dramatic improvement in the LIBs performance can be ascribed to the highly conductive

graphene sheets, the 3D hierarchical structure and the amorphous carbon layer.

Acknowledgment

This work was supported by National Basic Research Program of China (No.2009CB930000) and NSF of China (No. 20934002, 51073043)

Notes and references

1. M. Armand and J. M. Tarascon, *Nature*, 2008, **451**, 652-657.
2. J. M. Tarascon and M. Armand, *Nature*, 2001, **414**, 359-367.
3. P. G. Bruce, B. Scrosati and J.-M. Tarascon, *Angew. Chem. Int. Ed.*, 2008, **47**, 2930-2946.
4. G. Derrien, J. Hassoun, S. Panero and B. Scrosati, *Adv. Mater.*, 2007, **19**, 2336-2340.
5. J. Wang, J. Liu, D. Chao, J. Yan, J. Lin and Z. X. Shen, *Adv. Mater.*, 2014, **26**, 7162-7169.
6. Z. Wang, L. Zhou and X. W. Lou, *Adv. Mater.*, 2012, **24**, 1903-1911.
7. F. Cheng, Z. Tao, J. Liang and J. Chen, *Chem. Mater.*, 2008, **20**, 667-681.
8. D. Kong, H. He, Q. Song, B. Wang, W. Lv, Q.-H. Yang and L. Zhi, *Energy Environ. Sci.*, 2014, **7**, 3320-3325.
9. T. Yang and B. Lu, *Phys. Chem. Chem. Phys.*, 2014, **16**, 4115-4121.
10. X. W. Lou, D. Deng, J. Y. Lee, J. Feng and L. A. Archer, *Adv. Mater.*, 2008, **20**, 258-262.
11. X. Guan, J. Nai, Y. Zhang, P. Wang, J. Yang, L. Zheng, J. Zhang and L. Guo, *Chem. Mater.*, 2014, **26**, 5958-5964.
12. L. Taberna, S. Mitra, P. Poizot, P. Simon and J. M. Tarascon, *Nat. Mater.*, 2006, **5**, 567-573.
13. W. Yang, G. Cheng, C. Dong, Q. Bai, X. Chen, Z. Peng and Z. Zhang, *J. Mater. Chem. A*, 2014, **2**, 20022-20029.
14. J.-H. Jeun, K.-Y. Park, D.-H. Kim, W.-S. Kim, H.-C. Kim, B.-S. Lee, H. Kim, W.-R. Yu, K. Kang and S.-H. Hong, *Nanoscale*, 2013, **5**, 8480-8483.
15. N. Balke, S. Jesse, A. N. Morozovska, E. Eliseev, D. W. Chung, Y. Kim, L. Adamczyk, R. E. Garcia, N. Dudney and S. V. Kalinin, *Nat. Nanotechnol.*, 2010, **5**, 749-754.
16. J. Lee, S.-H. Yu, C. Kim, Y.-E. Sung and J. Yoon, *Phys. Chem. Chem. Phys.*, 2013, **15**, 7690-7695.
17. Y. Lou, J. Liang, Y. Peng and J. Chen, *Phys. Chem. Chem. Phys.*, 2015, **17**, 8885-8893.
18. Z. Zhang, F. Wang, Q. An, W. Li and P. Wu, *J. Mater. Chem. A*, 2015, **3**, 7036-7043.
19. Z. Zhang, L. Zhang, W. Li, A. Yu and P. Wu, *ACS Appl. Mater. Interfaces*, 2015, **7**, 10395-10400.
20. Y. Xia, W. Zhang, Z. Xiao, H. Huang, H. Zeng, X. Chen, F. Chen, Y. Gan and X. Tao, *J. Mater. Chem.*, 2012, **22**, 9209-9215.
21. X. Liu, S. W. Or, C. Jin, Y. Lv, C. Feng and Y. Sun, *Carbon*, 2013, **60**, 215-220.
22. D. Xie, Q. Su, W. Yuan, Z. Dong, J. Zhang and G. Du, *J. Phys. Chem. C*, 2013, **117**, 24121-24128.
23. X. Xu, H. Tan, K. Xi, S. Ding, D. Yu, S. Cheng, G. Yang, X. Peng, A. Fakeeh and R. V. Kumar, *Carbon*, 2015, **84**, 491-499.
24. S. H. Choi, Y. N. Ko, J.-K. Lee and Y. C. Kang, *Sci. Rep.*, 2014, **4**.
25. G. Zhou, D.-W. Wang, L.-C. Yin, N. Li, F. Li and H.-M. Cheng, *ACS nano*, 2012, **6**, 3214-3223.
26. X. Sun, C. Yan, Y. Chen, W. Si, J. Deng, S. Oswald, L. Liu and O. G. Schmidt, *Adv. Energy Mater.*, 2014, **4**, 1300912-1300918.
27. H. Long, T. Shi, H. Hu, S. Jiang, S. Xi and Z. Tang, *Sci. Rep.*, 2014, **4**, 7413-7422.
28. S. Tao, W. Yue, M. Zhong, Z. Chen and Y. Ren, *ACS Appl. Mater. Interfaces*, 2014, **6**, 6332-6339.
29. D.-H. Lee, J.-C. Kim, H.-W. Shim and D.-W. Kim, *ACS Appl. Mater. Interfaces*, 2014, **6**, 137-142.
30. V. Aravindan, P. S. Kumar, J. Sundaramurthy, W. C. Ling, S. Ramakrishna and S. Madhavi, *J. Power Sources*, 2013, **227**, 284-290.
31. S. A. Needham, G. X. Wang and H. K. Liu, *J. Power Sources*, 2006, **159**, 254-257.
32. Y. Zou and Y. Wang, *Nanoscale*, 2011, **3**, 2615-2620.
33. M. Sasidharan, N. Gunawardhana, C. Senthil and M. Yoshio, *J. Mater. Chem. A*, 2014, **2**, 7337-7344.
34. L. Zhuo, Y. Wu, W. Zhou, L. Wang, Y. Yu, X. Zhang and F. Zhao, *ACS Appl. Mater. Interfaces*, 2013, **5**, 7065-7071.
35. H. Huang, T. Feng, Y. Gan, M. Fang, Y. Xia, C. Liang, X. Tao and W. Zhang, *ACS Appl. Mater. Interfaces*, 2015, **7**, 11842-11848.
36. X. Yang, Y.-B. Tang, X. Huang, H. T. Xue, W. P. Kang, W. Y. Li, T.-W. Ng and C.-S. Lee, *J. Power Sources*, 2015, **284**, 109-114.
37. W. Yue, S. Jiang, W. Huang, Z. Gao, J. Li, Y. Ren, X. Zhao and X. Yang, *J. Mater. Chemistry A*, 2013, **1**, 6928-6933.
38. W. S. Hummers and R. E. Offeman, *J. Am. Chem. Soc.*, 1958, **80**, 1339-1339.
39. Y. Ni, Y. Yin, P. Wu, H. Zhang and C. Cai, *ACS Appl. Mater. Interfaces*, 2014, **6**, 7346-7355.
40. X. Wang, L. Qiao, X. Sun, X. Li, D. Hu, Q. Zhang and D. He, *J. Mater. Chem. A*, 2013, **1**, 4173-4176.
41. S.-X. Wang, S. Chen, Q. Wei, X. Zhang, S. Y. Wong, S. Sun and X. Li, *Chem. Mater.*, 2015, **27**, 336-342.
42. Y. J. Mai, S. J. Shi, D. Zhang, Y. Lu, C. D. Gu and J. P. Tu, *J. Power Sources*, 2012, **204**, 155-161.
43. V.-D. Dao, L. L. Larina, K.-D. Jung, J.-K. Lee and H.-S. Choi, *Nanoscale*, 2014, **6**, 477-482.
44. J. Liang, H. Hu, H. Park, C. Xiao, S. Ding, U. Paik and X. W. Lou, *Energy Environ. Sci.*, 2015, **8**, 1707-1711.
45. R. A. Susantyoko, X. Wang, Q. Xiao, E. Fitzgerald and Q. Zhang, *Carbon*, 2014, **68**, 619-627.
46. W.-M. Zhang, X.-L. Wu, J.-S. Hu, Y.-G. Guo and L.-J. Wan, *Adv. Funct. Mater.*, 2008, **18**, 3941-3946.
47. X. Q. Yu, Y. He, J. P. Sun, K. Tang, H. Li, L. Q. Chen and X. J. Huang, *Electrochem. Commun.*, 2009, **11**, 791-794.
48. M. Yu, A. Wang, Y. Wang, C. Li and G. Shi, *Nanoscale*, 2014, **6**, 11419-11424.

49. X.-Y. Yu, H. Hu, Y. Wang, H. Chen and X. W. Lou, *Angew. Chem. Int. Ed.*, 2015, **54**, 7395-7398.
50. L. Zhang and X. W. Lou, *Chem. A Euro. J.*, 2014, **20**, 5219-5223.